Metastable phase diagram of Bi probed by single-energy x-ray absorption detection and angular dispersive x-ray diffraction

E. Principi, M. Minicucci, and A. Di Cicco
CNISM and Dipartimento di Fisica, Università degli Studi di Camerino, via Madonna delle Carceri 9, 62032 Camerino (MC), Italy

A. Trapananti, S. De Panfilis, and R. Poloni
European Synchrotron Radiation Facility, Boîte Postale 220, F-38043 Grenoble, France

(Received 2 May 2006; published 2 August 2006)

In this paper we report the results of a detailed experimental study of samples composed of micrometric Bi droplets providing an insight into the metastable phase diagram of Bi. To this purpose we have used the single-energy x-ray absorption detection technique in combination with angular dispersive x-ray diffraction available at the BM29 beamline of the European Synchrotron Radiation Facility. This unconventional approach has given proof of being a different and reliable tool for detecting subtle structural modifications in condensed matter. The investigation has revealed a large variety of metastable Bi polymorphs in a broad range of pressures and temperatures (25–500 °C, 0–6 GPa) and the occurrence of a Bi crystalline structure isomorphic to the β-tin structure. We have shown that the range of undercooling of liquid Bi strongly depends upon pressure and the underlying solid stable and metastable phases. As a final result a Bi-phase diagram including metastable phases is proposed, which takes into account all structural information obtained from this experiment.

DOI: 10.1103/PhysRevB.74.064101 PACS number(s): 61.10.Ht, 61.10.Nz, 64.60.My, 64.30.+t

I. INTRODUCTION

Bismuth (Bi) is a metal of the V group well known for exhibiting a large number of polymorphic transitions within a limited region of pressures and temperatures.[1–10] Bi crystallizes at moderate pressures and temperatures in open structures, which can be regarded locally as distorted simple-cubic lattices.[11–14] This atomic arrangement, typical of elements of the V group, is mainly due to the external electronic configuration (s^2p^3), which promotes covalent bonding by the p electrons spread along the three Cartesian axes.[11,14] The spatial localization of electrons induced by covalent bonding makes Bi a "poor metal" and it favors an open local environment. The presence of a locally open structure is favored also in the ambient pressure liquid phase, which has been found to have a low coordination number ($N<9$).[11,15] This value differs from the typical coordination number of pure liquid metals ($10<N<12$), suggesting possible structural similarities with covalent liquids like Si (group IV)[16–18] and Se (group VI).[13,19] The partial covalent bonding and the relativistic effects caused by its nuclear mass[20] strongly affect the Bi response to pressure and temperature determining a more complex behavior respect to the isovalent elements and other pure metals. The most striking characteristic is evidently the large negative slope of the melting curve in the low-pressure region ($P<1.7$ GPa).

The unusual structural characteristics observed in Bi, are common within a class substance (such as water, Si, Ge, Ga, Sb, GaSb, InSb, InAs,…) termed "ice-type," which is at the present time an object of great interest within the scientific community.[21] These materials show a relatively low density at low pressures, because of their open-packed local structures, but they easily experience phase transitions toward denser spatial arrangements under the action of pressure. Moreover, the polymorphism observed in the stable solid phases is suspected to affect also the liquid phase. Also, liquid Bi has been found to undergo resistivity anomalies at high pressures and temperatures.[22] Such unusual behavior of Bi and ice-type substances is understood in terms of a "two-fluid model" in which two different local atomic arrangements coexist in the liquid.[23–25] These are a low-density liquid (LDL) which locally resembles the low-pressure solid phase structure, and a high-density liquid (HDL) which can be associated with the structure of the high-pressure solid polymorphs. The relative concentration of these two fluids varies upon pressurization and this change could be associated with a liquid-liquid phase transition as observed in liquid P.[26] This holds also for metastable liquids. In fact, liquids can be strongly undercooled in the region of stability of a low-density solid phase, and a LDL-HDL transition may occur even in this metastable regime.

In this scenario the investigation of the metastable region of Bi becomes extremely attractive. Solid Bi exhibits a wide set of local atomic arrangements in a limited range of pressures and temperatures and it is a natural candidate for manifesting polymorphism also in the metastable phases. The aim of this study was to obtain information on the atomic structure of metastable Bi in a broad range of temperatures and pressures (25–500 °C, 0–6 GPa) investigating for structural anomalies and possible unknown atomic arrangements both in the liquid and in the solid phase. For this purpose we have exploited an advanced experimental setup installed at the BM29 beamline of the European Synchrotron Radiation Facility (ESRF) combining x-ray absorption spectroscopy (XAS) and angular dispersive x-ray diffraction (ADXD). These techniques are often used separately, limiting the sensitivity to the short-range order (XAS) or to the long-range order (ADXD). The present study confirms the importance of their combination to provide a complete and reliable determination of the atomic arrangement upon structural modifications induced by extreme pressure and temperature conditions.

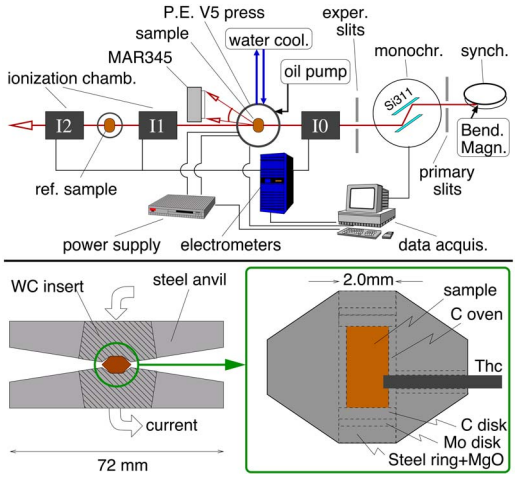

FIG. 1. (Color online) Upper panel: Layout of the advanced experimental setup available at BM29 (ESRF) improved for simultaneous SEXAD and ADXD measurements at high pressures and temperatures. Lower panel: Position of the boron-epoxy gasket between the anvils and electrical current flow (on the left). Transverse section of the boron-epoxy gasket used in this experiment (on the right) showing the internal parts and the thermocouple (Thc).

The contents of this paper are organized as follows: Sec. II is devoted to the experimental details. We describe the sample preparation, the experimental apparatus, and the principles of the single-energy x-ray absorption detection (SEXAD) technique. In Sec. III we present the results. Finally, in Secs. IV and V we discuss the findings and report the main conclusions.

II. EXPERIMENT

A. Setup

The experiment was carried out at the BM29 beamline of ESRF, which makes available a fully automated environment and an experimental setup specialized in high-quality XAS measurements.[27,28] The requested beam stability, intensity, and dimensions have been guaranteed by a double-crystal Si(311) Kohzu monochromator and by the advanced feedback system in use at BM29.[27] A sketch of the experimental setup used in this work is drawn in the upper panel of Fig. 1.

In order to collect ADXD patterns, a MAR345 image plate detector has been mounted in an off-axis position with respect to the beam at about 50 cm after the sample. A similar setup has been shown to be highly efficient at performing reliable and fast structural characterizations by x-ray diffraction (XRD) combined with energy dispersive XAS measurements.[29]

The image plate position and the selected energy ($E=15$ KeV, $\Delta E/E \approx 10^{-5}$) for ADXD measurements have been chosen in order to optimize the detection of the most intense Debye-Sherrer rings and kept fixed during the whole experimental run. The sample-detector distance has been calibrated using a Ag foil at the sample position. The horizontal experimental slits positioned in front of the sample (at about 50 cm) have been fixed at 0.5 mm, obtaining a full width at half maximum (FWHM) of about 0.1 degrees in the 2θ scale. It is worth noting that the width of the experimental slits has been increased during SEXAD measurements up to 1 mm to raise the photon counts.

A "Paris-Edinburgh" (PE) large volume (V5) press[30,31] positioned over an *xyz*-translation stage has been used as a pressure device. It can reach sample pressures up to about 10 GPa with standard WC anvils and it can heat the sample up to about 2000 °C by means of a 200 A power supply. Moreover, during the recording operation of the imaging plate (600 s) the press rotates continuously at ±2.5° around its symmetry axes orthogonal to the x-ray beam. This oscillation improves the powder statistics limited by the small dimensions of the sample and the x-ray spot.[28]

B. Sample preparation

High-purity Bi_2O_3 powder (99.999%) from Aldrich has been finely grounded and accurately dispersed in a suitable quantity of BN in order to optimize the x-ray absorption at the Bi L_3-edge (13 419 eV). The mixture has been pressed and the resulting pellet heated up to 700 °C in a vacuum chamber to obtain a complete reduction of the Bi oxide into the metal. We verified the full reduction of the original oxide both by a qualitative analysis of the x-ray absorption near-edge structure (XANES) of the sample and by x-ray diffraction. The deoxidized pellet has been crushed into a fine powder and a small quantity of NaCl has been added as a pressure marker. The final mixture was made in a weight ratio of Bi:NaCl:BN 1:2:30. This dilution has been found to guarantee negligible chemical reactions between NaCl and Bi and to avoid the formation of Bi droplets' aggregates. Powder mixtures prepared by using this technique have been found by scanning electron microscopy to be a dispersion of micrometric grains of the sample powder into the matrix, allowing the achievement of appreciable undercooling ranges still retaining the behavior of bulk samples due to the relatively large dimensions.[32]

In Fig. 1 (lower panel) the transverse section of a gasket used in this experiment is drawn which shows the detail of the internal small parts. The powder fills completely a hollow graphite cylinder which serves to heart the sample. The electrical contact between the graphite furnace and the anvils is guaranteed by two graphite disks which close the furnace, two Mo disks, and two steel rings filled by a MgO powder. All the gaskets have been drilled for insertion of an insulated 0.5 mm thermocouple. The high pressure upon the gasket is obtained by raising the pressure of an oil line (up to 1000 bar) by means of a manual pump. The special shape of gasket and anvils is designed to generate a quasihydrostatic pressure upon the sample. In order to reach high temperatures an electrical power supply is connected to the anvils. The electrical line is closed by the graphite furnace where the major part of the heating power is dispersed. The heat absorbed by the anvils and by the PE press is dispersed by a water cooling line which is connected to the press itself.

A crystalline Bi powder sample has been used as a room temperature-pressure reference sample between the second and the third ionization chambers (see Fig. 1, upper panel).

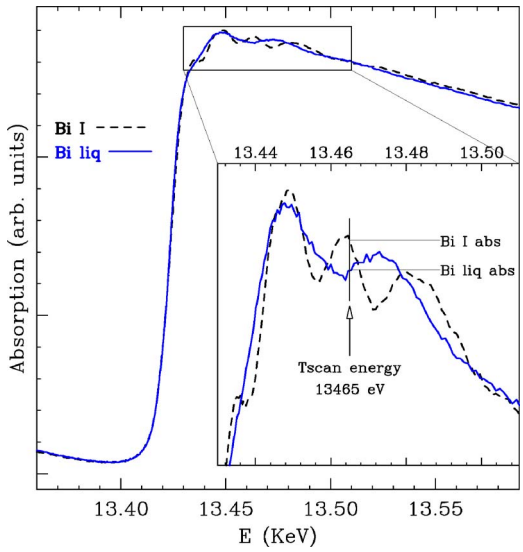

FIG. 2. (Color online) Typical XAS profiles of our samples near the Bi L_3-edge of Bi-I (dashed lines) at RT and liquid Bi (solid lines) at about 280 °C at room pressure. Inset: Detail of the near-edge structures where the differences in the shape of the x-ray absorption spectra are clearly visible. The absorbances of Bi-I and liquid Bi at 13 465 eV are indicated by horizontal lines.

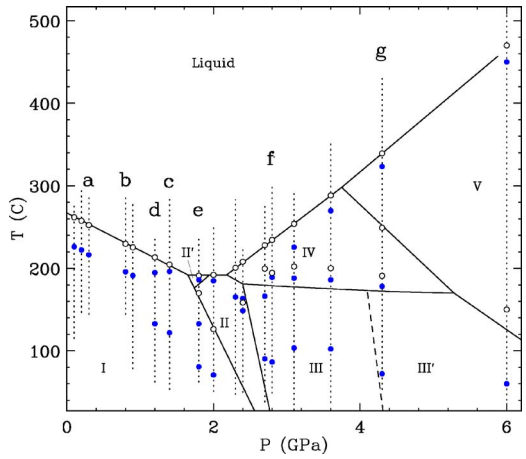

FIG. 3. (Color online) Phase diagram of Bi [adapted from Chen *et al.* (Ref. 8)] compared to the results of the *T*-scan analysis presented in this paper. The different phases are labeled following Cannon (Ref. 41). The vertical dotted lines, which join circles, represent the range of temperatures covered by the *T*-scan loop carried out at a given pressure. The phase transitions revealed by the *T* scans upon raising the temperature are represented by empty circles, while full circles indicate a phase transition upon cooling. The labels "a," "b," "c," "d," "e," "f," and "g" indicate the *T*-scan loops shown in Figs. 4–6.

The optimal sensitivity to the x-ray absorption at the Bi L_3-edge energy has been obtained filling the ionization chambers with 2 bar of a gas mixture of Ar and He ($I0$: P_{Ar}=0.3 bar, $I1$: P_{Ar}=1.0 bar, $I2$: P_{Ar}=1.5 bar) and selecting the suitable dynamical range of the electrometers connected to the chambers.

C. Techniques and procedure

The SEXAD and ADXD techniques have been used for the investigation of a broad region of the Bi-phase diagram.

The basic principle of the SEXAD technique is based on the occurrence of discontinuous changes of the shape of the x-ray absorption spectra upon a first-order phase transition.[33] As an example the L_3-edge x-ray absorption spectra of Bi-I and liquid Bi are shown and compared in Fig. 2. In the magnified inset of Fig. 2, two different levels of absorption associated with the two different Bi phases are observable at the energy of 13 465 eV. By monitoring the sample absorption at a fixed energy as a function of temperature (but also ideally other sample environmental parameters, such as pressures or magnetic fields could be varied), the occurrence of a transition can be detected with high accuracy by both raising or decreasing the temperature, collecting a set of reproducible SEXAD "hysteresis" loops hereafter called temperature scans or *T* scans. A crucial parameter of this technique is the energy value, which should be tuned in order to maximize the absorption changes and enhance the sensitivity to the observed phase transitions. One of the major advantages of this technique is its fast and precise response to structural modifications that is an important feature for investigating subtle metastable phases.

After the observation of one or more absorption discontinuities at a given pressure, the information provided by a *T* scan has been complemented by an accurate analysis of x-ray diffraction patterns. In particular the use of x-ray diffraction is fundamental for validating the SEXAD information in the presence of complex structural modifications. Moreover, the x-ray diffraction is necessary for estimating the sample pressure following the lattice contraction of internal pressure markers. Modern x-ray spectrometers today available, such as the BM29 beamline, are equipped with powerful monochromators which can be coupled with ease to an imaging plate for carrying out ADXD measurements. The presence of the imaging plate does not affect the XAS data acquisition and it is possible to change from XAS to ADXD in a few seconds without moving the sample and the imaging plate.

The measurements were repeated on three different samples following this experimental protocol: (i) a pressure increase up to a desired value; (ii) a beam alignment with the sample and the recording of an ADXD diffraction pattern at 15 KeV for calibrating the pressure; (iii) the selection of a suitable beam energy for the *T*-scan loops; (iv) a collection of several fixed x-ray energy *T* scans; (v) the collection of XAS spectra (Bi L_3 edge: 13 419 eV) and ADXD scans at suitable temperatures close to absorption discontinuities suspected to be structural phase transitions. The overall set of *T* scans carried out at fixed pressure during the experiment is shown in Fig. 3.

III. RESULTS

The phase transitions revealed by the *T* scans upon raising the temperature are represented in Fig. 3 by empty circles, whereas the full circles indicate the occurrence of a phase transition upon cooling. More details show that, at a given pressure, empty circles at the highest temperatures corre-

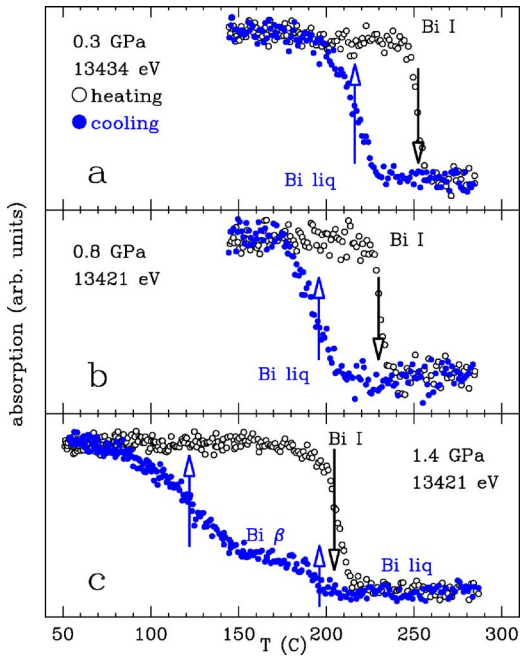

FIG. 4. (Color online) T scans of micrometric Bi droplets at fixed energy and pressure. The arrows indicate the temperature of the phase transitions, which corresponds to the temperature value of the circles in Fig. 3. The melting is associated with a sudden decrease of the absorbance. The cooling part in loop "c" differs from "a" and "b" for the presence of an intermediate plateau which is associated with the growth of a metastable solid phase (Bi β).

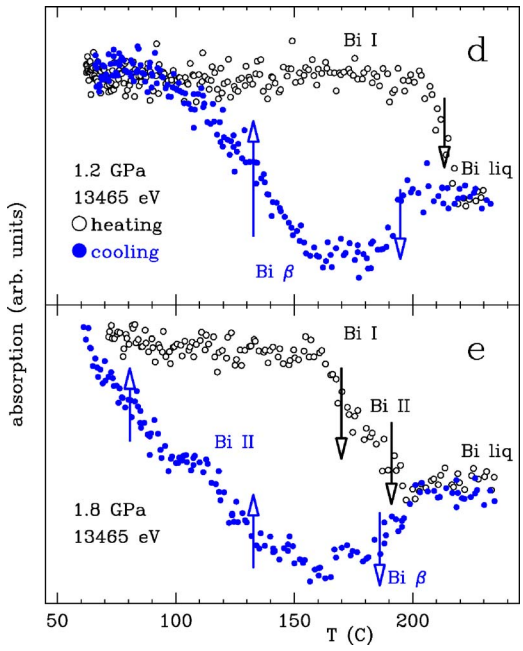

FIG. 5. (Color online) T scans of micrometric Bi droplets at fixed energy and pressure. The arrows indicate the temperature of the phase transitions, associated with the temperature value of the circles in Fig. 3. The loop "d" reveals the same information obtained from the loop "c" of Fig. 4, but it has different shape because of the different energy. As expected observing the inset in Fig. 2, the absorbance level of the liquid phase is lower than that of Bi-I. The loop "e" carried out at the same energy, but at higher pressure, presents two plateaus both upon heating and cooling at an intermediate level of absorption. These features in the T-scan profile are due to the stable phase Bi-II.

spond to the melting of the sample, while full circles represent the freezing points and the transformation from a metastable solid to a stable or metastable solid. The vertical dotted lines, joining the circles in Fig. 3, show the range of temperatures covered by a T-scan loop at a given pressure. Published melting curves[8] were taken as a reference for the present investigation, scaling our temperature readout accordingly. The measured temperatures were found in agreement with published values within 20 °C.

Next, seven typical T scans will be discussed. They are displayed in Figs. 4–6 and labeled with letters from "a" to "g" to identify their pressure and temperature ranges in Fig. 3. The vertical arrows in Figs. 4–6 indicate the estimated transition temperatures and they have been set at the half-height value of the absorption discontinuities. In Fig. 4 the scans "a," "b," and "c" have been collected at 13 434 and 13 421 eV, close to the L_3 edge of Bi, respectively, at P =0.3, 0.8, and 1.4 GPa. The scans show a sudden drop of absorbance occurring upon melting. A typical hysteresis loop is visible, indicating the occurrence of a metastable liquid phase.[32–34] The Bi melting curve has negative slope for increasing pressure up to about 2 GPa and indeed the melting transition temperature decreases with pressurization (a shift of the black arrows in Fig. 4). The crystallization temperature of the undercooled liquid follows the same trend, but an anomaly occurs at 1.4 GPa, as shown by the T scan "c." The cooling part of the loop "c" differs from "a" and "b" because of the presence of an intermediate plateau, noticeable upon undercooling of the liquid phase. The range of undercooled liquid is drastically reduced at this pressure. This feature is associated with the appearance of a metastable (not detected upon heating) phase which manifests itself within the Bi-I region of stability. In what follows we call this metastable phase "β-Bi." The presence of β-Bi is noticeable also in the T scans "d" and "e" collected at 1.2 and 1.8 GPa, respectively, and displayed in Fig. 5. T scans "d" and "e" have been carried out at a different energy (14 465 eV) more suitable for enhancing the sensitivity to the β-Bi phase. Similar to the T scan c, we observe hardly any undercooling in the T scans "d"and "e" as liquid Bi rapidly crystallizes in β-Bi. In particular in the T scan "e," the temperature range where the liquid Bi is undercooled collapses completely. Moreover, the loop "e" contains further interesting features not observable in the loop "d." It presents two plateaus at the same absorbance level both upon heating and cooling, indicating the occurrence of another stable phase (Bi-II).

ADXD patterns were collected to confirm the information provided by the above-described T-scan profiles. In Fig. 7 four typical ADXD patterns are presented as recorded on the MAR345 image plate with an exposure time of 600 s. They were collected at about 1.8 GPa upon cooling at the following temperatures: 220 °C (liquid Bi), 180 °C (first plateau), 110 °C (second plateau), and room temperature (solid Bi-I) as found by the T scan "e" in Fig 5. Four Bragg patterns have been obtained by radial integration and are shown in Fig. 8. They confirm that the changes of absorption revealed by

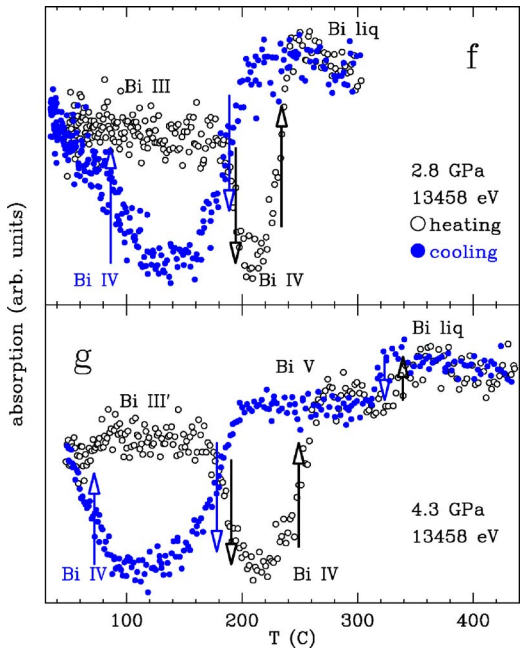

FIG. 6. (Color online) T scans of micrometric Bi droplets at fixed energy and pressure. The arrows indicate the temperature of the phase transitions, corresponding to the position of the circles in Fig. 3. The energy has been selected to enhance the absorbance differences among Bi high-pressure polymorphs. All the phases obtained upon heating appear upon cooling.

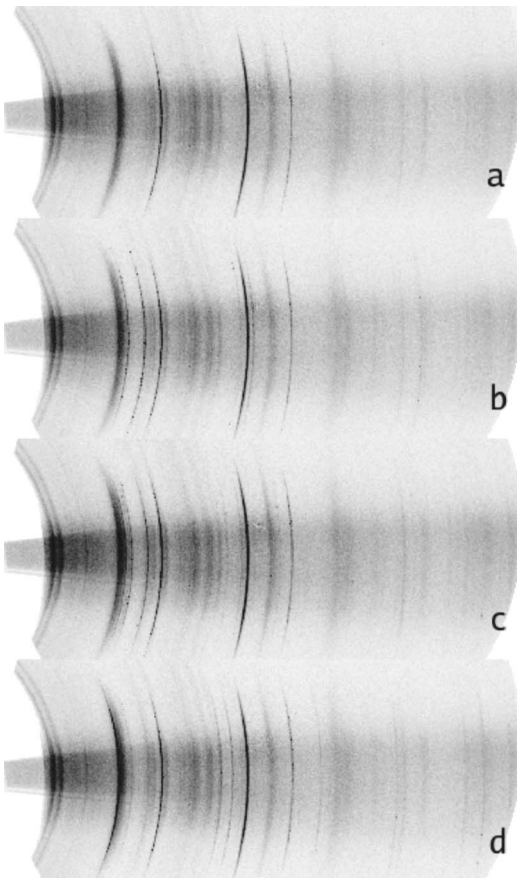

FIG. 7. ADXD digital images recorded on the MAR345 imaging plate at 1.8 GPa at four different temperatures. (a) $T=220$ °C: liquid Bi; (b) $T=180$ °C: β-Bi; (c) $T=110$ °C: Bi-II; (d) room temperature: Bi-I. The typical Debye-Sherrer rings are generated by the mixture Bi:NaCl:BN with a ratio of 1:2:30. The incoming x-ray beam energy is 15 KeV with an energy resolution $\Delta E/E \approx 10^{-5}$. The total exposure time is 600 s.

SEXAD correspond to three different Bi crystal structures. The Bragg peaks positions associated with the β-Bi structure at 180 °C are compatible with a β-tin type structure (cell parameters: $a \simeq 6.210$ Å, $b \simeq 3.311$ Å). At 110 °C Bi crystallizes in the Bi-II phase (cell parameters: $a \simeq 6.716$ Å, $b \simeq 6.126$ Å, $c \simeq 3.314$ Å, $\beta \simeq 111.0°$) and finally at room temperature into Bi-I with a residual part of Bi-II. To our knowledge a β-tin structure for solid Bi has never been observed before. Both β-Bi and Bi-II have the same number of atoms in the unit cell ($Z=4$) (Ref. 35) and similar coordination numbers ($N_\beta \simeq 6$, $N_{II} \simeq 7$), suggesting a similar local atomic arrangement. A possibility is that β-Bi could be the structure of the so-called Bi-II′ phase which has been so far revealed only by the differential thermal analysis (DTA) technique[37,36] and whose atomic structure is still unknown.[38] The stability region of Bi-II′ is restricted to a small region of the phase diagram at about 1.9 GPa and 190 °C, but the structural information provided by this experiment points out that a larger metastable region of Bi-II′ can exist at lower pressures and temperatures.

Figure 6 presents T scans "f" and "g" performed, respectively, at about 2.8 and 4.3 GPa. Within this region of pressures, Bi has a positive slope of the melting line. The sequence of polymorphs that appeared upon heating is in accord with the Bi-stable phase diagram. Upon cooling several interesting structural features are noticeable. The undercooling range observed by T scan "f" is drastically reduced in T scan "g." This effect should be related to the different crystalline structures contiguous to the stable liquid. In fact the nucleation process is favored in a liquid which locally resembles the underlying crystalline atomic arrangement, otherwise it is retarded because the undercooled state is usually kinematically favored.[39] Therefore we could infer that the local atomic structure of the high pressure liquid Bi is more similar to the Bi-V structure body centered cubic (bcc) than to the Bi-IV structure (monoclinic, $N=8$).

IV. DISCUSSION

In Fig. 9 a phase diagram including the appearance of metastable phases of Bi is finally proposed, which takes into account the structural information provided by the SEXAD and ADXD techniques.

Our experiment has revealed that above 1 GPa the metastable liquid crystallizes into the metastable structure β-Bi (see Fig. 9), which has been found to have a β-tin crystalline structure. This change is accompanied by a marked reduction of the size of the undercooling region which decreases to vanish completely at the triple point (I-II-L). In Fig. 9 the coexistence line between metastable liquid Bi and metastable β-Bi follows as a continuation of the stable Bi-II melting line. It could be conjectured that the Bi-II melting line continues through the region of stability of Bi-I up to ambient

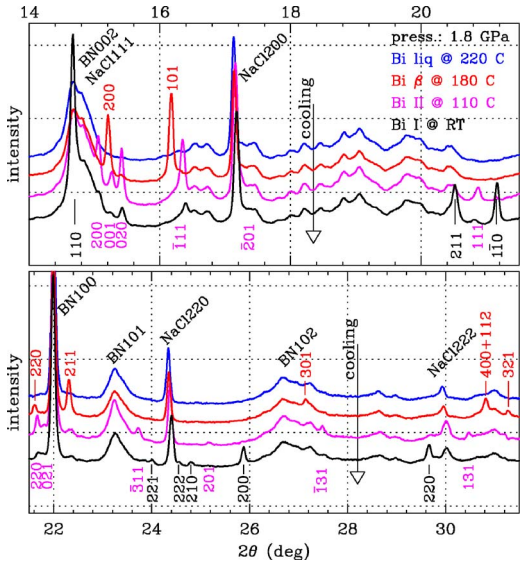

FIG. 8. (Color online) Diffraction patterns of the mixture Bi:NaCl:BN at a ratio of 1:2:30 at 220 °C, 180 °C, 110 °C and room temperature ($P=1.8$ GPa) as obtained from the imaging plate measurements shown in Fig. 7. The angular range shown is $\Delta(2\theta)=17.5°$ (upper panel $14°<2\theta<21.5°$, lower panel $21.5°<2\theta<31.5°$). Diagonal labels indicate peaks due to the BN matrix and to the pressure marker (NaCl). Vertical labels are the Miller indexes of β-Bi (top), Bi-II (middle), Bi-I (bottom).

pressure, influencing the structural behavior of undercooled liquid Bi. As suggested by Tanaka,[21] below such a line the undercooled liquid could fall in a region of competing ordering between two different liquids where hidden liquid-liquid transitions are highly probable. Unfortunately, below 1 GPa an undercooling of about 40 °C has been obtained which has been followed by the crystallization in the Bi-I solid stable phase, obscuring possible structural changes in the metastable phases.

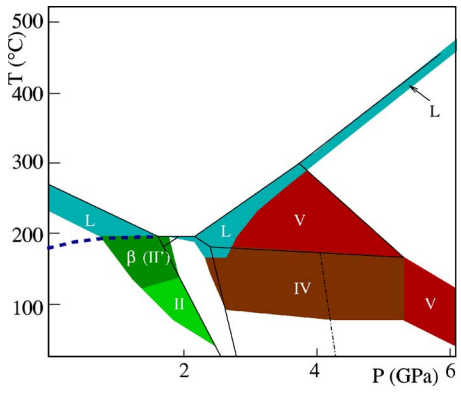

FIG. 9. (Color online) Metastable phase diagram of micrometric Bi droplets obtained from analyzing the temperature of the phase transitions upon cooling reported in Fig. 3. The different phases are labeled following Cannon (Ref. 41). The solid lines indicate the Bi stable phase diagram adapted from Chen *et al.* (Ref. 8). The dashed line below 2 GPa mimics the melting line of metastable solid Bi proposed by Yoon *et al.* (Ref. 40). In this paper the metastable phase β and stable phase II′ are proposed to be isostructural.

Our results are consistent with previous differential scanning calorimetry (DSC) and differential thermal analysis (DTA) measurements carried out by Yoon *et al.*[40] which have been able to undercool micrometric Bi droplets at ambient pressure up to 56 °C. The authors claimed the discovery of the melting line of the metastable solid phase Bi-II at low pressures (0–0.5 GPa). Yoon *et al.*[40] extrapolate their data collected close to the ambient pressure drawing a slightly convex line (similar to an isothermal) which starts at about 174 °C and 0 GPa and ends at the triple point (I-II-L). This curve is represented by a dashed line in Fig. 9 and is in excellent agreement with the metastable liquid Bi crystallization line revealed by our T scans between 1 and 2 GPa. SEXAD-ADXD and previous DSC-DTA information put into evidence the presence of a transition line inside the stability region of Bi-I which affects the structural behavior of the Bi metastable phases.

Finally, we want to focus attention on the anomalous behavior of the metastable phases represented in Fig. 9. A first anomaly can be observed at about 2 GPa. Around that pressure undercooling vanishes, but it can be obtained again at about 2.5 GPa. This is probably caused by the complexity of the stable Bi-phase diagram. A possible explanation can be that both low-density Bi-I and high-density Bi-IV have local structures and densities which differ from that of the liquid, allowing for a greater undercooling. On the other hand at about 2 GPa the local atomic arrangement of liquid Bi could be more compatible ($N\sim7$) with that of the underlying β-Bi and Bi-II. Moreover, around 2 GPa the density of liquid Bi in the vicinity of its crystallization line is comparable to the densities of β-Bi and Bi-II as obtained by the Clausius-Clapeyron equation. This can favor nucleation of the liquid around 2 GPa.

Another striking effect is observable between 3 and 4 GPa. Within that region of pressures liquid Bi does not crystallize in the Bi-IV phase as expected observing the stable phase diagram, but it nucleates in the Bi-V phase, which is metastable in that region. Again, this behavior could be assigned to the structural similarities between liquid Bi and Bi-V (BCC) above 3 GPa. The change toward Bi-IV takes place only in the region of stability of Bi-III, generating another metastable crystal which survives up to about 100 °C.

V. CONCLUSIONS

We have reported an accurate and challenging study of the metastable phase diagram of Bi in a broad range of pressures and temperatures (25–500 °C, 0–6 GPa), carried out exploiting the unique features of synchrotron radiation sources combined with single-energy x-ray absorption detection (SEXAD) and angular dispersive x-ray diffraction (ADXD). The SEXAD technique has been used to reveal the temperatures of the structural phase transitions at given pressures. The ADXD patterns recorded by the imaging plate have been used to determine the structural characteristics of the solid Bi polymorphs and pressure markers. The required pressures and temperatures have been reached by means of a large volume "Paris-Edinburgh" V5 press which can be easily

combined with the SEXAD and ADXD techniques. This advanced experimental approach guarantees a great accuracy for detecting subtle structural phase changes and is a reliable tool for investigating matter under extreme conditions.

We have shown that the range of undercooling of liquid Bi strongly depends upon pressure and the underlying solid stable and metastable phases. The nucleation of metastable liquid Bi is retarded when the underlying crystal has different local structure and density. This could explain the presence of undercooling in Bi-I and Bi-IV, respectively, below 2 GPa and around 2.5 GPa. On the contrary, Bi nucleation is very fast if the liquid is isomorphic to the crystalline structure as observed at about 2 GPa.

Metastable liquid Bi has been found to crystallize into metastable solid structures such as β-Bi at about 2 GPa and Bi-V between 3 and 4 GPa. The β-Bi solid phase is compatible with a β-tinlike structure, and it may be identified as the metastable phase of the so-called Bi-II' structure. Finally, in accord with previous nonstructural investigations, we have shown the presence of a transition line within the region of stability of Bi-I which affects the structural behavior of metastable phases.

Several questions are still open on the structural effects which may affect the Bi metastable liquid in the low-pressure region (<1 GPa). A further step could be to undercool deeply the liquid Bi below 180 °C at room pressure to carry out an accurate structural study. This could offer an important extension of the results presented here. We believe that this paper will stimulate the realization of new investigations on the Bi-metastable-phase diagram and will add other interesting arguments to the debate on polymorphism in ice-type substances under extreme conditions.

ACKNOWLEDGMENTS

We are grateful to G. Aquilanti for the help in setting up the experimental apparatus and for useful advice in running the MAR345 ADXD detector.

[1] F. P. Bundy, Phys. Rev. **110**, 314 (1958).
[2] W. Klement, Jr., A. Jayaraman, and G. C. Kennedy, Phys. Rev. **131**, 632 (1963).
[3] S. Nichols, J. Phys. D **5**, 799 (1972).
[4] S. Nichols, J. Phys. D **5**, 1898 (1972).
[5] H. Iwasaki, J. H. Chen, and T. Kikegawa, Rev. Sci. Instrum. **66**, 1388 (1995).
[6] J. H. Chen, H. Iwasaki, and T. Kikegawa, High Press. Res. **15**, 143 (1996).
[7] J. H. Chen, H. Iwasaki, and T. Kikegawa, J. Phys. Chem. Solids **58**, 247 (1997).
[8] J. H. Chen, T. Kikegawa, O. Shimomura, and H. Iwasaki, J. Synchrotron Radiat. **4**, 21 (1997).
[9] A. Di Cicco, L. Comez, J.-P. Itié, and A. Polian, in AIRAPT-17 Proceedings, Honolulu, Hawaii, 2000, edited by M. H. Manghnani, W. J. Nellis, and M. F. Nicol, p. 452.
[10] M. I. McMahon, O. Degtyareva, and R. J. Nelmes, Phys. Rev. Lett. **85**, 4896 (2000).
[11] K. Tsuji, J. Non-Cryst. Solids **117–118**, 27 (1990).
[12] D. A. Young, *Phase Diagrams of the Elements* (University of California Press, Berkeley, CA, 1991).
[13] Y. Katayama and K. Tsuji, J. Phys.: Condens. Matter **15**, 6085 (2003).
[14] K. Yaoita, K. Tsuji, Y. Katayama, M. Imai, and J.-Q. Chen, J. Non-Cryst. Solids **150**, 25 (1992).
[15] Y. Waseda, *The Structure of Non-Crystalline Materials* (McGraw-Hill, New York, 1980).
[16] N. Jakse, L. Hennet, D. Price, S. Krishnan, T. Key, E. Artacho, B. Glorieux, A. Pasurel, and M.-L. Saboungi, Appl. Phys. Lett. **83**, 4734 (2003).
[17] C. A. Angell and S. Borick, J. Phys.: Condens. Matter **11**, 8163 (1999).
[18] S. Ansell, S. Krishnan, J. J. Felten, and D. L. Price, J. Phys.: Condens. Matter **10**, L73 (1999).
[19] V. V. Brazhkin and A. G. Lyapin, J. Phys.: Condens. Matter **15**, 6059 (2003).
[20] W. B. Holzapfel, Rep. Prog. Phys. **59**, 29 (1996).
[21] H. Tanaka, Phys. Rev. B **66**, 064202 (2002).
[22] V. V. Brazhkin, S. V. Popova, and R. N. Voloshin, High Press. Res. **15**, 267 (1997).
[23] E. Rapoport, J. Chem. Phys. **46**, 2891 (1967).
[24] L. I. Aptekar, Sov. Phys. Dokl. **24**, 993 (1979).
[25] E. G. Ponyatovsky, J. Phys.: Condens. Matter **15**, 6123 (2003).
[26] Y. Katayama, T. Mizutani, W. Utsumi, O. Shimomura, M. Yamakata, and K. Funakoshi, Nature (London) **403**, 170 (2000).
[27] A. Filipponi, M. Borowski, D. T. Bowron, S. Ansell, A. Di Cicco, S. De Panfilis, and J.-P. Itiè, Rev. Sci. Instrum. **71**, 2422 (2000).
[28] A. Filipponi, V. M. Giordano, S. D. Panfilis, A. Di Cicco, E. Principi, A. Trapananti, M. Borowski, and J.-P. Itiè, Rev. Sci. Instrum. **74**, 2654 (2003).
[29] G. Aquilanti, W. Crichton, and S. Pascarelli, High Press. Res. **23**, 301 (2003).
[30] J. M. Besson, R. J. Nelmes, G. Hamel, J. S. Loveday, G. Weill, and S. Hull, Physica B **180&181**, 907 (1992).
[31] L. G. Khvostantsev, V. N. Slesarev, and V. V. Brazhkin, High Press. Res. **24**, 371 (2004).
[32] L. Ottaviano, A. Filipponi, and A. Di Cicco, Phys. Rev. B **49**, 11749 (1994).
[33] A. Filipponi, M. Borowski, P. W. Loeffen, S. De Panfilis, A. Di Cicco, F. Sperandini, M. Minicucci, and M. Giorgetti, J. Phys.: Condens. Matter **10**, 235 (1998).
[34] A. Filipponi, A. Di Cicco, and S. De Panfilis, Phys. Rev. Lett. **83**, 560 (1999).
[35] R. M. Brugger, R. B. Bennion, and T. G. Worlton, Phys. Lett. **24A**, 714 (1967).
[36] E. Y. Tonkov, *High Pressure Phase Transformations, A Handbook* (Gordon and Breach Science Publishers, New York, 1992), Vol. 1.
[37] D. Decker, J. Jorgensen, and R. Young, High Temp. - High Press. **7**, 331 (1975).
[38] J. L. Pélissier and N. Wetta, Physica A **289**, 459 (2001).
[39] D. Turnbull, in *Undercooled Alloy Phases*, edited by E. W. Collings and C. C. Koch (Metallurgical Society, Warrandale, PA, 1987).
[40] W. Yoon, J. S. Paik, D. LaCourt, and J. H. Perepezko, J. Appl. Phys. **60**, 3489 (1986).
[41] J. F. Cannon, J. Phys. Chem. Ref. Data **3**, 781 (1974).